Spin Hall effect in noncollinear kagome antiferromagnets

Oliver Busch,* Börge Göbel, and Ingrid Mertig
Institut für Physik, Martin-Luther-Universität Halle-Wittenberg, D-06099 Halle (Saale), Germany

(Received 30 August 2021; accepted 9 November 2021; published 18 November 2021)

The spin Hall effect is commonly considered to be related to spin-orbit interaction that causes a deflection of charge carriers according to their spin orientation into opposite directions. Thus, this effect creates spin currents in nonmagnetic materials with spin-orbit coupling. However, recently large spin Hall effects were predicted in coplanar kagome antiferromagnets Mn_3X even when spin-orbit interaction is not considered. Therefore, these materials are interesting candidates for spintronic applications. In our theoretical study we reveal two sources that determine the intrinsic spin Hall signal of two-dimensional kagome antiferromagnets. The main contribution to the spin Hall signal is originating from the noncollinear magnetic texture localized on the Mn sites and it is maximal for coplanar systems. In addition to that, spin-orbit coupling or an out-of-plane tilting of the magnetic moments, which are equivalent within the framework of this model, reduce the spin Hall effect effectively.

DOI: 10.1103/PhysRevB.104.184423

I. INTRODUCTION

Conventionally only the charge of electrons is used in electronic devices like transistors, displays, or solar panels [1]. However, in the emerging field of spintronics [2,3] the spin degree of freedom of the electrons is as well exploited [4,5]. Therefore, the investigation of materials, with regard to manipulation and control of spin and generation of spin currents, is mandatory for the development of new low-power consumption applications [6,7]. Besides, spin-based electronics can build on a wide range of different materials like metals [8], semiconductors [9–12], or superconductors [13] that have all been taken into account for application in spintronics devices for the last decades.

Spin currents are generated in metals by the spin Hall effect as a transverse response to a longitudinal electrical field [8,14,15]. In experiments, this effect can be quantified by a transverse accumulation of spin density with opposite sign at the edges that can be measured directly via the magneto-optical Kerr effect (MOKE) [16]. Alternatively, the spin Hall effect can be quantified by a spin Hall conductivity which is measured indirectly by exploiting the inverse spin Hall effect where the spin current is converted back into a transverse charge current [17]. A propagation of such spin currents across a metal/ferromagnet interface allows for magnetization switching via spin-orbit torque [18]. The same scenario holds for collinear antiferromagnets [cf. Fig. 1(a)]. Spin-polarized currents typically occur in ferromagnetic materials. Longitudinal spin-polarized currents are for example responsible for effects like the giant magnetoresistance and spin-transfer torque [19,20] which are utilized in magnetic RAMs [21]. Transversal spin-polarized currents are related to the anomalous Hall effect [cf. Fig. 1(b)].

Recently, materials with antiferromagnetic order gained attention. Although the observation and manipulation of antiferromagnetic textures and domains is much more challenging in experiments and applications [22,23], they show interesting properties like a strong robustness against external magnetic fields and the absence of magnetic stray fields [5]. Moreover, they allow for ultrafast spin dynamics and magnetotransport phenomena [24,25].

A special type of antiferromagnets is considered in this work: noncollinear magnetic textures on a two-dimensional kagome lattice. This structure can be found in some manganese compounds Mn_3X (X = Rh, Ir, Pt, Ga, Ge, Sn) that are constituted by layered kagome planes [26] where the magnetic moments of the Mn atoms form a noncollinear antiferromagnetic texture. These materials have been the subject of many recent theoretical and experimental studies about the anomalous and the spin Hall effect, where spin-orbit interaction plays an important role.

The anomalous Hall effect has been predicted [26–28] in these noncollinear kagome magnets and confirmed in experiments with Mn_3Sn [29] and Mn_3Ge [30,31]. Besides, Zhang *et al.* showed that in such compensated systems large spin Hall effects may occur as well [26], and most interestingly, even when spin-orbit coupling is not considered. Time-reversal symmetry $\mathcal{T}$ is broken in magnetic systems, whereas a combination of $\mathcal{T}$ with a spin rotation $\mathcal{S}$ by 180° around the axis perpendicular to the kagome plane can still be a symmetry. This $\mathcal{TS}$ symmetry forbids the existence of the anomalous Hall effect in a noncollinear coplanar magnetic texture but the spin Hall effect can exist, even without spin-orbit interaction [32].

The symmetry analysis is a powerful tool, however, it does not allow for a quantitative prediction of the size of the effect. There are cases where the magnetic space group of a crystalline material would allow for the existence of an anomalous Hall effect [32,33], but the effect can be absent, as was shown before in Ref. [34]. There we established a

*Corresponding author: oliver.busch@physik.uni-halle.de

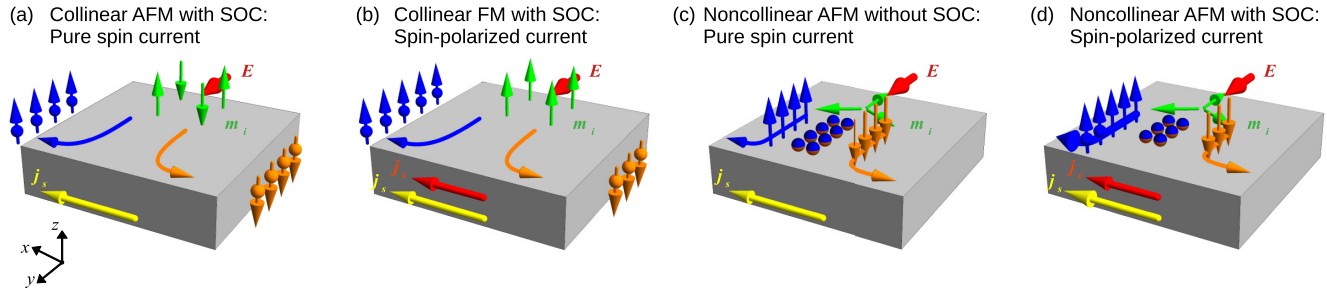

FIG. 1. Overview of spin currents and spin-polarized currents in different magnetic systems. Green arrows represent the magnetic texture $\{\boldsymbol{m}_i\}$ [of the Mn atoms in (c) and (d)]. The thick red arrows indicate the electric field $\boldsymbol{E}$ along y. The electrons participating in transport are distinguished according to their spin orientation in z direction (blue: ↑, orange: ↓). The small spheres represent the charge of the electrons. (a) Collinear antiferromagnet (AFM) with spin-orbit coupling (SOC): pure transverse spin current $\boldsymbol{j}_s$ (yellow arrow) since electrons with different spin accumulate at opposite sites of the sample and no charge current $\boldsymbol{j}_c$ can be measured. (b) Collinear ferromagnet (FM) with SOC where not only spin but also charge is transported (thin red arrow), resulting in a spin-polarized charge current. (c) Noncollinear AFM without SOC: In contrast to the situation in (a), spin currents (yellow arrow) may exist even without spin-orbit interaction. (d) Same as (c) but with SOC that gives rise to an anomalous Hall effect in addition. Therefore, charge currents may flow in addition in analogy to the situation in (b).

microscopic picture that allows us to interpret the anomalous Hall effect in Mn_3X systems as an effective topological Hall effect: spin-orbit interaction induces a virtual tilting of the magnetic moments out of the kagome plane. Thus, the opening angle of this virtual noncoplanar texture generates an effective topological Hall effect due to a net scalar spin chirality, whereas the magnetic background texture formed by the magnetic moments of the Mn atoms remains coplanar.

In this work we are investigating the spin Hall effect [8,14,15] in the same model system and relate the findings to our previous results of the anomalous Hall effect and the virtual magnetic texture. We find that the spin Hall signal is determined by two different mechanisms. First, a large spin Hall effect emerges from the coplanar magnetic background texture itself that is independent of the in-plane rotation of the magnetic moments. In addition to that, spin-orbit coupling or an out-of-plane tilting of the magnetic moments, which is equivalent within this model, is related to a spin-polarized current that reduces the spin Hall signal of the background texture effectively. This allows us to distinguish pure spin currents, where only spin is transported by the electrons, and spin-polarized currents, where spin and charge are transported, as a transverse response to an applied electric field in those systems.

Hence, we find analogies between noncollinear kagome magnets and collinear (anti-)ferromagnets as illustrated in Fig. 1. Without spin-orbit interaction a pure spin current is flowing in coplanar kagome magnets [cf. Fig. 1(c)] like in a collinear antiferromagnet [cf. Fig. 1(a)]. Taking spin-orbit coupling into account causes additionally a spin-polarized current that is related to an anomalous Hall effect which reduces the spin Hall conductivity [cf. Fig. 1(d)]. The spin-polarized current is similar to the situation in a collinear ferromagnet [cf. Fig. 1(b)].

Although we stress the analogy of collinear antiferromagnets and noncollinear kagome antiferromagnets with respect to the generation of spin currents, there is a pronounced difference. Collinear bipartite antiferromagnets [35] show an analogy of Kramer's theorem since the time-reversal operation $\mathcal{T}$ in combination with a translation between the sublattices T_d are a symmetry in the system. Consequently, the bands are doubly degenerate and the corresponding eigenvectors can be classified into "spin-up" and "spin-down" states [cf. blue and orange small spheres in Fig. 1(a)]. There is no symmetry in kagome antiferromagnets that fulfills Kramer's theorem: the bands are not doubly degenerate [27]. However, the corresponding eigenvectors consist of equal contributions of spin-up and spin-down with respect to the quantization axis perpendicular to the kagome plane, which is illustrated by the two-colored small spheres in Fig. 1(c). Hence, each eigenstate generates a pure spin current on its own. Spin-orbit coupling is changing the equal distribution of spin-up and spin-down character. As a result an individual state still contributes to the spin current, however somewhat reduced, and delivers an appropriate amount of spin-polarized current as well [cf. Fig. 1(d)].

II. MODEL AND METHODS

The model Hamiltonian that we use was first introduced in Ref. [27] where the anomalous Hall effect has been predicted in the compensated kagome magnet Mn_3Ir. It is also known as an *sd* model that describes the interaction of itinerant s electrons with d magnetic moments that are localized on the Mn sites and form a noncollinear magnetic texture. In second quantization, the tight-binding Hamiltonian reads

$$H = H_\mathrm{kin} + H_\mathrm{Z} + H_\mathrm{SOC}, \tag{1}$$

$$H_\mathrm{kin} = t \sum_{\langle i,j\rangle} \sum_{\sigma} a^\dagger_{i,\sigma} a_{j,\sigma}, \tag{2}$$

$$H_\mathrm{Z} = m \sum_{i} \sum_{\sigma,\sigma'} a^\dagger_{i,\sigma} (\boldsymbol{m}_i \cdot \boldsymbol{\sigma})_{\sigma\sigma'} a_{i,\sigma'}, \tag{3}$$

$$H_\mathrm{SOC} = i\lambda \sum_{\langle i,j\rangle} \sum_{\sigma,\sigma'} a^\dagger_{i,\sigma} (\boldsymbol{n}_{ij} \cdot \boldsymbol{\sigma})_{\sigma\sigma'} a_{j,\sigma'}, \tag{4}$$

where $a^\dagger_{i,\sigma}$ and $a_{i,\sigma}$ are the creation and annihilation operators of an electron at site i with spin σ. Here we restrict ourselves to nearest-neighbor hopping between atomic sites i and j which is implied by the sum limits $\langle i, j\rangle$. The three parameters t, m, and λ denote the hopping energy, the strength of the Hund's coupling between the spin moment of the conduction

electron with the magnetic texture $\boldsymbol{m} = \{\boldsymbol{m}_i\}$, and the strength of spin-orbit interaction, respectively. Here

$$\boldsymbol{m}_i = \begin{pmatrix} \cos(\Phi_i)\sin(\theta_i) \\ \sin(\Phi_i)\sin(\theta_i) \\ \cos(\theta_i) \end{pmatrix} \tag{5}$$

is the magnetic moment at site i characterized by the polar and azimuthal angles Φ_i and θ_i and the vectors $\boldsymbol{n}_{ij}$ are defined in Ref. [34] [cf. Fig. 1(a)]. These in-plane vectors $\boldsymbol{n}_{ij}$ form a set of vectors that are anticlockwise orthogonal to the hopping vectors $\boldsymbol{R}_{ij}$ which consider the different environments (left or right hand) of nearest-neighbor hoppings on a kagome lattice [27].

In our study the kagome lattice, which is a two-dimensional hexagonal lattice with a triangular unit cell (formed by Mn atoms), is located in the xy plane and is assumed to be periodic. The considered tight-binding model allows for a continuous rotation of the magnetic moments $\boldsymbol{m}_i$, that are carried by Mn atoms, within and out of the kagome plane. Following the notation from Ref. [34], the different magnetic textures can be characterized as follows. First of all, only magnetic textures with a positive vector spin chirality [36]

$$\kappa \equiv \frac{2\sqrt{3}}{9} \sum_{\langle i,j \rangle} (\boldsymbol{m}_i \times \boldsymbol{m}_j) \cdot \boldsymbol{e}_z = +1 \tag{6}$$

are considered. Rotating each magnetic moment by the same in-plane offset angle $\Delta\Phi$ within the xy plane, as visualized in the small cartoons in Fig. 4, does not change the vector spin chirality since the magnetic moments of neighboring atoms always differ by a polar angle of 120°.

Two configurations are special since they have different symmetries (time reversal $\mathcal{T}$, mirror reflection $\mathcal{M}$): "radial" ($\Delta\Phi = 0°$, three $\mathcal{TM}$ planes) and "toroidal" ($\Delta\Phi = 90°$, three $\mathcal{M}$ planes). We always assume that all three magnetic moments have the same azimuthal angle $\theta \equiv \theta_i$ for a certain magnetic texture. Thus, coplanar and noncoplanar configurations are classified by an azimuthal angle of $\theta = 90°$ and $\theta \neq 90°$, respectively, in this work.

We investigate the influence of the spin configuration on the spin Hall effect. Within linear response theory, the corresponding spin Hall conductivity σ_{ij}^k is a tensor of rank three and relates an electric field E_j (applied in j direction) to the spin current $j_{s,i}^k = \sigma_{ij}^k E_j$ that is generated as a response flowing in i direction with spin polarization in k direction ($i, j, k = x, y, z$). We focus on the intrinsic contribution which can be described by the Berry curvature formalism analog to the intrinsic anomalous Hall conductivity [37]. For a two-dimensional system at zero temperature, as considered here, the intrinsic spin Hall conductivity is defined as follows [26]:

$$\sigma_{xy}^z(E_\mathrm{F}) = \frac{e}{\hbar} \sum_\nu \frac{1}{(2\pi)^2} \int_{\varepsilon(\boldsymbol{k}) \leqslant E_\mathrm{F}} \Omega_{xy,\nu}^z(\boldsymbol{k})\, d^2k, \tag{7}$$

where the Fermi energy E_F enters as a parameter that can be varied in practice by doping or by applying a gate voltage. In this equation, the Brillouin zone integration is performed over all occupied states for a quantity that is sometimes denoted as "spin Berry curvature" [26,32]

$$\Omega_{xy,\nu}^z(\boldsymbol{k}) = -2\hbar^2\, \mathrm{Im} \sum_{\mu \neq \nu} \frac{\langle \nu, \boldsymbol{k} | \Sigma_x^z | \mu, \boldsymbol{k} \rangle \langle \mu, \boldsymbol{k} | v_y | \nu, \boldsymbol{k} \rangle}{[\varepsilon_\nu(\boldsymbol{k}) - \varepsilon_\mu(\boldsymbol{k})]^2} \tag{8}$$

of band ν that is calculated from the eigenvalues $\varepsilon_\nu(\boldsymbol{k})$ and the corresponding eigenvectors $|\nu, \boldsymbol{k}\rangle \equiv \varphi_\nu(\boldsymbol{k})$ of the tight-binding Hamiltonian. In contrast to the conventional Berry curvature, here one has to take into account the spin-current operator that can be defined by $\Sigma_i^k \equiv \frac{1}{2}\{v_i, s^k\}$ as the anticommutator of the velocity operator v_i and the spin operator s^k.

III. RESULTS AND DISCUSSION

The results section of our paper is organized as follows: we investigate the influence of the in-plane and out-of-plane orientation of the magnetic moments on the intrinsic spin Hall effect by systematically varying the parameters $\Delta\Phi$ and θ, respectively. Thereby we observe pure spin currents without spin-orbit coupling that cause the spin Hall signal. Spin-orbit interaction brings about spin-polarized currents, as well, that reduce the spin Hall signal effectively.

A. Spin Hall effect for the radial and toroidal coplanar configurations

Throughout this subsection the fixed magnetic texture is assumed to be coplanar ($\theta = 90°$) and the parameter describing the Hund's coupling is set to $m = 1.7\,t$.

First, the radial configuration ($\Delta\Phi = 0°$) is investigated without taking spin-orbit interaction into account ($\lambda = 0.0\,t$). Figures 2(a) and 2(b) show the corresponding band structure where one obtains six individual bands and Dirac points at K due to the $\mathcal{TM}$ symmetry of the magnetic texture [27]. The color of the energy bands represents the spin Berry curvature $\Omega_{xy,\nu}^z$ in units of a^2, where a is the lattice constant. A detailed $\boldsymbol{k}$- and band-resolved plot of the spin Berry curvature in Fig. 2(c) illustrates that $\Omega_{xy,\nu}^z$ has finite values (green positive, yellow zero, and red negative) allowing for the occurrence of the spin Hall effect even though spin-orbit coupling is not considered, as predicted by Zhang *et al.* [32]. The corresponding spin Hall conductivity σ_{xy}^z according to Eq. (7) is plotted in units of $(\frac{e^2}{\hbar})(\frac{\hbar}{e})$ as a function of energy simulated by a change of the Fermi energy E_F [black curve in Fig. 3(b)] which is in agreement with Ref. [32]. Note that this result corresponds to the situation illustrated for the sample in Fig. 1(c).

Now we take spin-orbit interaction into account ($\lambda = 0.2\,t$). Therefore, we briefly summarize the main results of our former work about the virtual magnetic texture that explains the anomalous Hall effect in this scenario [34].

We demonstrated via a transformation of the model Hamiltonian (1) that spin-orbit coupling and a tilting of the magnetic texture out of the kagome plane are equivalent.

The application of a set of unitary transformations that tilt the local z axis at each lattice site i by the same angle α towards the magnetic moment $\boldsymbol{m}_i$ implies that one can change the reference system to a lattice-site dependent coordinate

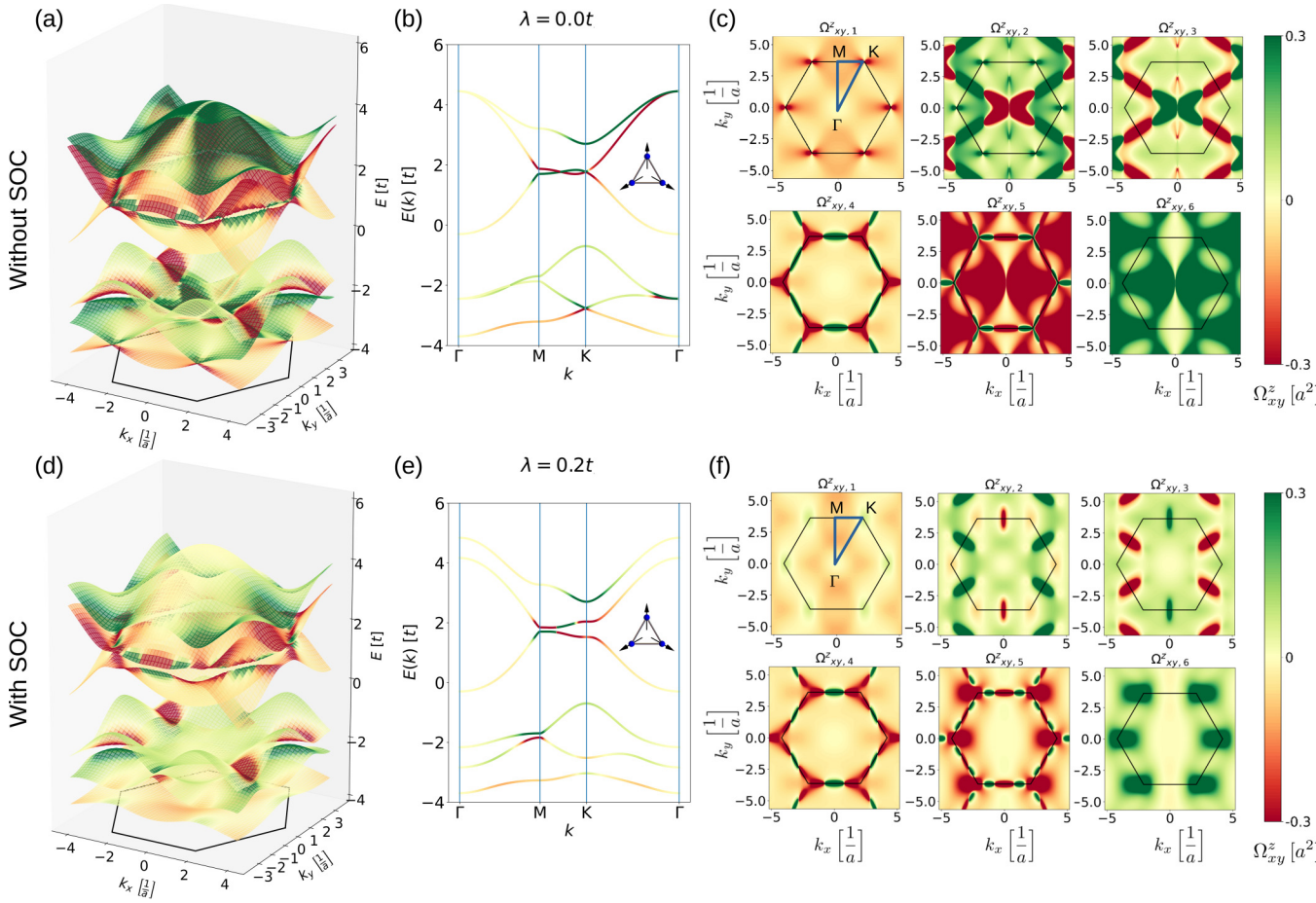

FIG. 2. Band structure and spin Berry curvature of the radial magnetic texture. In (a)–(c) spin-orbit coupling (SOC) is neglected, whereas in (d)–(f) it is considered. (a) Three-dimensional band structure $E(k_x, k_y)$ for all bands over the Brillouin zone (indicated by the black hexagon in the k_x-k_y plane). The color of the energy surfaces shows the value of the spin Berry curvature Ω^z_{xy} (green positive, red negative, and yellow zero as indicated by the legend on the right). (b) Same as in (a) but represented in the reduced zone scheme where the band structure is only plotted along the high-symmetry points (Γ-M-K-Γ). (c) Visualization of the spin Berry curvature of all bands resolved in the two-dimensional k space. The blue triangle in the upper left panel in (c) shows the reduced Brillouin zone. (d)–(f) Analog to (a)–(c), but spin-orbit interaction is taken into account ($\lambda = 0.2\,t$).

system where the magnetic texture is effectively tilted by α:

$$\tilde{\boldsymbol{m}}_i = \begin{pmatrix} \cos(\Phi_i)\sin(\theta-\alpha) \\ \sin(\Phi_i)\sin(\theta-\alpha) \\ \cos(\theta-\alpha) \end{pmatrix}. \tag{9}$$

Besides, the unitary transformation of the complete Hamiltonian (1) yields effective hopping and spin-orbit coupling amplitudes $\tilde{t}$ and $\tilde{\lambda}$. For the radial configurations, the latter reads

$$\tilde{\lambda} = -\frac{\sqrt{3}}{2}\sin(\alpha)\,t + \cos(\alpha)\,\lambda. \tag{10}$$

This equation implies that the effective spin-orbit coupling can be compensated ($\tilde{\lambda} = 0$) by a critical tilting angle α_c. In this case, we call the effectively tilted magnetic texture $\{\tilde{\boldsymbol{m}}_i\}$ "virtual" and it is tilted with respect to the fixed magnetic texture $\boldsymbol{m} = \{\boldsymbol{m}_i\}$ by an azimuthal angle $\alpha_c = \Delta\theta_c$. In particular, Eq. (10) yields a critical angle $\alpha_c \approx 13^\circ$ for $\lambda = 0.2\,t$.

The virtual texture is hidden in the model Hamiltonian (1) and is thereby determined by the symmetry of the system. Consequently, the virtual texture is responsible for the electronic properties and thus, the equivalence of spin-orbit interaction and an out-of-plane tilting allows for an interpretation of the anomalous Hall effect in the coplanar kagome magnet ($\theta = 90^\circ$) as an effective topological Hall effect due to a nonvanishing scalar spin chirality of the virtual noncoplanar magnetic texture ($\tilde{\theta} = 90^\circ - \alpha_c$).

Moreover, a noncoplanar background texture $\{\boldsymbol{m}_i\}$ that is characterized by a critical azimuthal angle $\theta_c = 90^\circ + \Delta\theta_c$ with spin-orbit coupling ($\lambda \neq 0$) is equivalent to a virtual coplanar texture, since $\{\tilde{\boldsymbol{m}}_i\}$ is tilted by $\alpha_c = \Delta\theta_c$ with respect to $\{\boldsymbol{m}_i\}$. Hence, spin-orbit coupling is effectively compensated ($\tilde{\lambda} = 0$) and the Hall effect vanishes again since the already mentioned $\mathcal{TM}$ symmetry of the radial configuration, and thus of the Hamiltonian, is restored.

The out-of-plane tilting mechanism that arises from spin-orbit interaction is parameter dependent and the influence on the in-plane orientation of the magnetic moments is given by a cosine function [34]. Hence, it is maximal for the radial configuration and zero for the toroidal configuration which implies that the virtual texture is not tilted with respect to the original toroidal texture. The reason for this is that spin-orbit

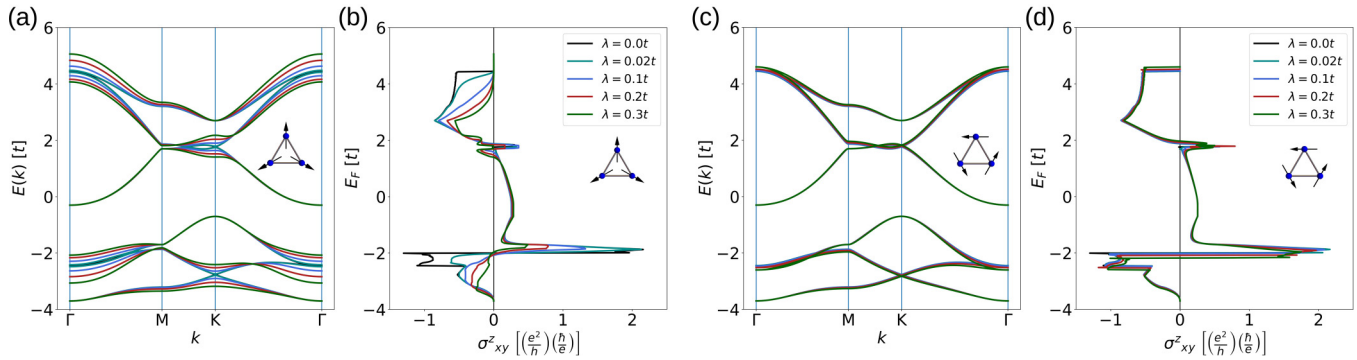

FIG. 3. Band structure and spin Hall conductivity σ^z_{xy} plotted against the Fermi level E_F for different spin-orbit coupling strengths λ as indicated. (a) and (b) show the results for the radial configuration ($\Delta\Phi = 0°$), where band gaps occur due to spin-orbit coupling and broaden with increasing λ, whereas the spin Hall signal is reduced for most energies. (c) and (d) show the results of analog calculations for the toroidal texture ($\Delta\Phi = 90°$) which is obtained by an in-plane rotation of each magnetic moment by 90° within the kagome plane.

coupling breaks the $\mathcal{TM}$ symmetry of the radial configuration ($\Delta\Phi = 0°$), whereas $\mathcal{M}$ in the toroidal arrangement ($\Delta\Phi = 90°$) is still conserved [27,36]. Note that the magnetic moments of textures with different in-plane orientations as discussed in Sec. III B can be interpreted as a superposition of a radial and a toroidal part. The tilting increases with the spin-orbit interaction strength λ.

Now we discuss the consequences of the virtual texture on the band structure and the spin Hall signal for the radial texture. Since spin-orbit coupling is considered, the $\mathcal{TM}$ symmetry of the magnetic texture is broken and therefore degeneracies are lifted and global band gaps open [cf. Fig. 2(e)]. In Fig. 3(a) the dependence of the electronic band structure on the spin-orbit interaction strength λ is presented. Figure 3(b) shows the corresponding spin Hall signals, where we find that the magnitude of the spin Hall conductivity is decreasing for most energies with increasing λ. For the red curve in Fig. 3(b) we set $\lambda = 0.2\,t$ in correspondence to Ref. [32].

According to Ref. [38], a phase transition from the radial phase ($\Delta\Phi = 0°$) to the toroidal phase ($\Delta\Phi = 90°$) has been found experimentally at a critical temperature $T_C = 163$ K in the antiperovskite Mn_3NiN. Repeating the calculations for the toroidal texture reveals that both the electronic structure and the spin Hall signal are hardly affected by spin-orbit coupling [cf. Figs. 3(c) and 3(d)]: the Dirac points do not open as band gaps but the bandwidth is slightly broadened with increasing λ.

B. Spin Hall effect under in-plane rotation of the magnetic moments

The electronic properties (i.e., the band structure and the spin Hall conductivity) without spin-orbit coupling (black curves in Fig. 3) are identical for the two special configurations, but the effect of spin-orbit interaction is quite strong for the radial phase and almost negligible for the toroidal one. Motivated by this, we investigate the spin Hall effect for configurations between those two arrangements. Since the band structures of the radial and the toroidal configurations can differ significantly, if spin-orbit coupling is taken into account [cf. Fig. 3(a)], it is helpful to calculate the conductivity as a function of the occupation number n_{occ} instead of the Fermi energy E_F to compare different systems with each other. Therefore, we calculate σ^z_{xy} upon a continuous variation of the in-plane offset angle $\Delta\Phi$ while n_{occ} is fixed.

As visible in Fig. 4(a), we find for each fixed occupation number that the spin Hall conductivity as a function of $\Delta\Phi$ is constant if spin-orbit interaction is not taken into account. This is in agreement with the above discussion of the spin transport in the radial and the toroidal configurations without spin-orbit coupling. The signal is independent of the in-plane orientation of the magnetic texture (illustrated by the small cartoons below the panel in Fig. 4). If spin-orbit interaction is taken into account ($\lambda = 0.2\,t$), we observe an extra contribution to the spin Hall signal that is oscillating with a period of 180° [cf. Fig. 4(b)]. This periodic behavior is in agreement with symmetry arguments since the (intrinsic) spin Hall conductivity, which is considered in this work, is even under time reversal $\mathcal{T}$ which is equivalent to a rotation of each magnetic moment by 180° in the kagome plane. Consequently, the spin Hall signal fulfills $\sigma^z_{xy}(\Delta\Phi + 180°) = \sigma^z_{xy}(\Delta\Phi)$.

The spin Hall conductivity for a fixed occupation can be strongly diminished depending on the in-plane orientation. The difference is maximal for the radial configuration and minimal for the toroidal one. To illustrate this more clearly, the spin Hall conductivity for those two magnetic textures and configurations in between are shown as a function of the occupation number in one diagram in Fig. 4(c) where the horizontal lines indicate the number of the occupied states that have been chosen for the in-plane rotation in Figs. 4(a) and 4(b).

C. Relation of spin Hall effect to anomalous Hall effect and magnetization density

Now we would like to interpret our results and relate them to the findings in Ref. [34] where the anomalous Hall effect has been investigated.

Without spin-orbit coupling, our calculations revealed that the anomalous Hall effect is absent and there is only a constant contribution to the spin Hall signal originating from the magnetic background texture. In this case there is only a pure spin current [cf. Fig. 1(c)]. As we will show in the following, the contribution which is arising from spin-orbit coupling and

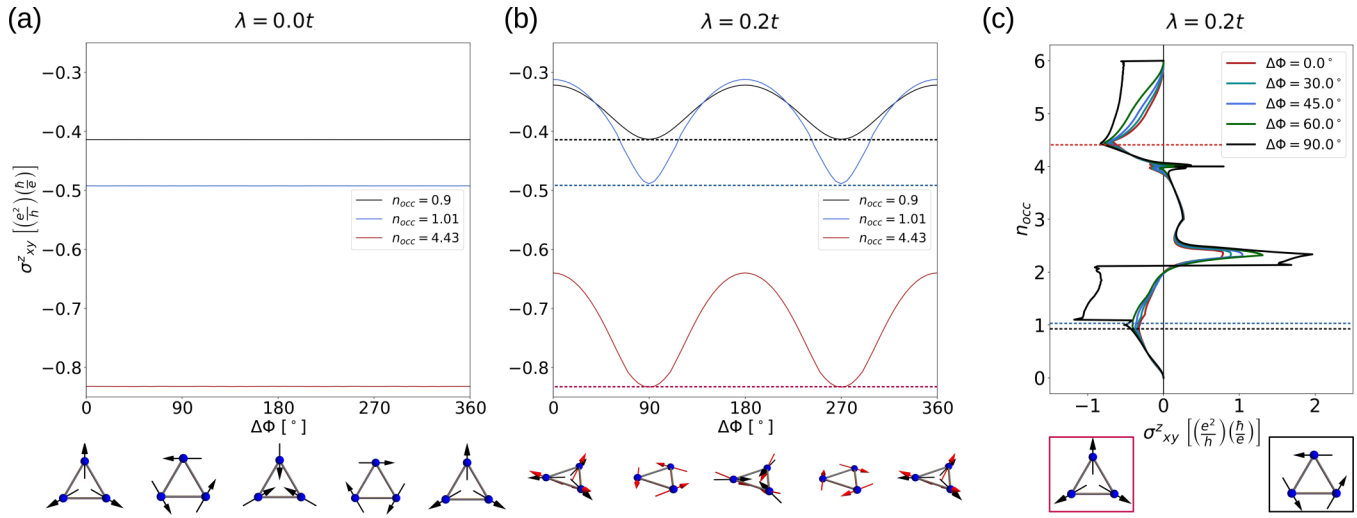

FIG. 4. Spin Hall conductivity for different fixed occupation numbers n_{occ} upon a continuous rotation of the magnetic moments within the kagome plane as indicated by the small cartoons below the panel. (a) Spin-orbit coupling is not taken into account and in this case the spin Hall signal is nonzero, but constant and thus independent of the in-plane orientation of the magnetic moments. (b) Same as (a) but spin-orbit interaction is considered ($\lambda = 0.2\,t$). Here the spin Hall conductivity is oscillating with a period of 180° and so does the out-of-plane component of the magnetic moments of the virtual texture (red arrows in the small cartoons). (c) σ^z_{xy} plotted against n_{occ} for the radial (red) and toroidal phase (black) and configurations in between the two with spin-orbit interaction taken into account [$\lambda = 0.2\,t$ as in (b)]. The horizontal lines indicate the values of the fixed occupation numbers in (a) and (b).

which is reducing the spin Hall signal is roughly proportional to the anomalous Hall conductivity σ_{xy} multiplied with the magnetization density μ^s_z,

$$\Delta\sigma^z_{xy}(\mathrm{SOC}) \propto \sigma_{xy}\,\mu^s_z. \tag{11}$$

We will demonstrate this now by examining the behavior of the systems while varying the parameter m that describes the Hund's coupling strength between the spin moment of the conduction electron and the magnetic texture $\{\boldsymbol{m}_i\}$. Therefore, we are calculating not only the spin Hall conductivity σ^z_{xy} but also the anomalous Hall conductivity σ_{xy} and the out-of-plane component of the magnetization density μ^s_z upon rotating the magnetic moments within the kagome plane, as before.

The calculation of σ_{xy} is performed via Kubo formalism [37]:

$$\sigma_{xy}(E_{\mathrm{F}}) = -\frac{e^2}{h}\sum_{\nu}\frac{1}{2\pi}\int_{\varepsilon(\boldsymbol{k})\leqslant E_{\mathrm{F}}}\Omega_{xy,\nu}(\boldsymbol{k})\,d^2k, \tag{12}$$

where one has to integrate over the conventional Berry curvature

$$\Omega_{xy,\nu}(\boldsymbol{k}) = -2\hbar^2\,\mathrm{Im}\sum_{\mu\neq\nu}\frac{\langle\nu,\boldsymbol{k}|v_x|\mu,\boldsymbol{k}\rangle\,\langle\mu,\boldsymbol{k}|v_y|\nu,\boldsymbol{k}\rangle}{[\varepsilon_\nu(\boldsymbol{k})-\varepsilon_\mu(\boldsymbol{k})]^2}. \tag{13}$$

The magnetization density can be calculated from the spin texture of the itinerant magnetic moments of the conduction electrons' spins in reciprocal space. The z component of the spin texture of band ν is obtained by the calculation of the spin expectation value

$$\left\langle s^z_\nu(\boldsymbol{k})\right\rangle = \langle\nu,\boldsymbol{k}|\sigma^z|\nu,\boldsymbol{k}\rangle\,, \tag{14}$$

where σ^z is the Pauli matrix. Integrating over all occupied states in the Brillouin zone and summing over all bands yields the out-of-plane component of the magnetization density

$$\mu^s_z = \mu_{\mathrm{B}}\sum_{\nu}\frac{1}{(2\pi)^2}\int_{\varepsilon(\boldsymbol{k})\leqslant E_{\mathrm{F}}}\left\langle s^z_\nu(\boldsymbol{k})\right\rangle d^2k. \tag{15}$$

The results for σ_{xy} (in units of $\frac{e^2}{h}$) and μ^s_z (in units of μ_{B}) are presented together with σ^z_{xy} in Fig. 5 where we set the occupation number $n_{\mathrm{occ}} = 0.9$.

Without spin-orbit interaction (cf. dashed lines), the anomalous Hall effect is prohibited and the spin texture is coplanar, whereas the spin Hall effect is constant. σ_{xy} and μ^s_z vanish identically, independent of m and the in-plane rotation. The amount of σ^z_{xy} is decreased with increasing m [39].

Taking spin-orbit interaction into account ($\lambda = 0.2\,t$, solid lines in Fig. 5), yields a cosinusoidal behavior [40] of both the anomalous Hall conductivity and the z component of the magnetization density as a function of $\Delta\Phi$, whereas the spin Hall conductivity oscillates with the half-period, as before in Fig. 4. Now, enlarging the strength of the Hund's coupling m causes not only a reduction of the amount of the spin Hall signal, but also of the out-of-plane magnetization density, i.e., the spin texture aligns more and more with the coplanar texture. The amplitude of σ_{xy} is hardly affected by m.

For the toroidal configurations ($\Delta\Phi = 90°, 270°$), the anomalous Hall effect is absent and the spin texture remains coplanar, protected by the $\mathcal{M}$ symmetry. Consequently, there is no reduction of the spin Hall signal [cf. Eq. (11)] and we would observe a pure spin current even upon considering spin-orbit coupling. For all other configurations, the product of the finite and cosinusoidal signals σ_{xy} and μ^s_z explains the reduction of the spin Hall signal which is oscillating with a period of 180°.

We interpret the nonvanishing out-of-plane magnetization and charge current emerging due to spin-orbit interaction as

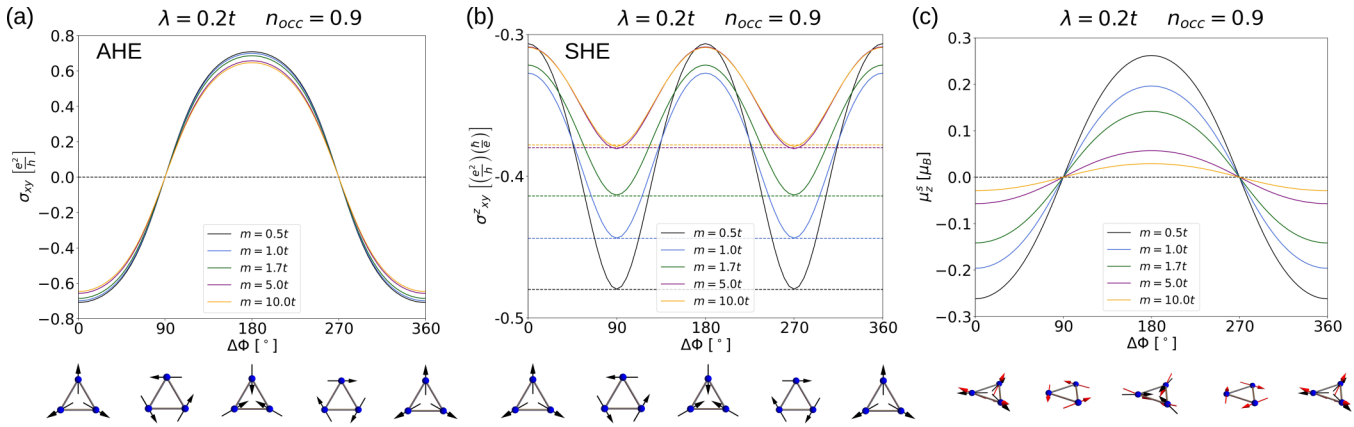

FIG. 5. Dependence of anomalous and spin Hall conductivity and the magnetization density on the Hund's coupling parameter m calculated for a fixed occupation number ($n_{\mathrm{occ}} = 0.9$) as a function of $\Delta\Phi$, analog to Fig. 4. For calculations with spin-orbit interaction (solid lines), we set $\lambda = 0.2\,t$. The dashed lines indicate the results of analog calculations without spin-orbit coupling. (a) The anomalous Hall conductivity σ_{xy} is only finite (and cosinusoidal) if spin-orbit coupling is taken into account. The anomalous Hall signal is only weakly reduced with increasing m and remains zero for the toroidal arrangements ($\Delta\Phi = 90°, 270°$). (b) Spin Hall conductivity σ^z_{xy} analog to Fig. 4(b). The amplitude of the contribution originating from the magnetic texture is reduced by spin-orbit coupling for all configurations except for the toroidal one. This additional contribution is shrinking with growing m. (c) Like σ_{xy}, the z component of the spin texture and thus the magnetization density μ^s_z is only nonzero if spin-orbit coupling is taken into account. As visible, the spin texture is continuously aligning with the real coplanar magnetic texture upon increasing Hund's coupling strength m. Note that μ^s_z remains zero for the toroidal configurations independent of λ and m.

a spin-polarized current. The latter is reducing the pure spin current of the magnetic background texture that causes the spin Hall effect, which is illustrated in Fig. 1(d).

D. Spin Hall effect under out-of-plane rotation of the magnetic moments

Summing up to this point, two different mechanisms contribute to the intrinsic spin Hall effect in noncollinear kagome antiferromagnets. One source is the Hund's coupling of the spin of the conduction electron to the chiral antiferromagnetic texture $\{\boldsymbol{m}_i\}$ itself where spin-orbit interaction is not required. The second contribution to the signal is mainly reducing the spin conductivity and it is originating from spin-orbit coupling that gives rise to a virtual magnetic texture $\{\tilde{\boldsymbol{m}}_i\}$. As explained before, the virtual texture determines the electronic properties and can be interpreted as tilting with respect to the real texture depending on the in-plane orientation $\Delta\Phi$ and on the spin-orbit coupling strength λ.

Motivated by these findings, magnetic textures that are already tilted out-of the kagome plane [$\theta \neq 90°$; cf. Eq. (5)] are investigated, in order to analyze the two contributions to the spin Hall signal. This could be achieved by applying an external magnetic field along z. However, we assume that the magnetic moments are only rotated and their magnitude does not change.

We calculate σ^z_{xy} for a fixed Fermi energy upon varying θ while $\Delta\Phi$ is constant [cf. small cartoons in Figs. 6(a) and 6(b)]. Since the tilting mechanism of the virtual magnetic texture is strongest for the radial arrangement, we set $\Delta\Phi = 0°$.

First of all, we discuss the results if we neglect spin-orbit interaction [cf. Fig. 6(a)]. For the collinear configurations ($\theta = 0°, 180°$), the spin Hall signal is zero since the spin Hall effect is absent in ferromagnets without spin-orbit coupling that would deflect electrons with different spin in opposite directions [41]. For all other configurations we get finite values and the spin Hall signal is completely symmetric with respect to $\theta = 90°$. In this case, the virtual magnetic texture is not tilted with respect to the real texture but the noncoplanar texture has an opening angle that gives rise to a pure topological Hall effect which implies that charge is transported as a response to an applied electric field. Since the spin Hall signal without spin-orbit interaction is independent of the in-plane rotation $\Delta\Phi$, it is worth noting that analog calculations for arbitrary $\Delta\Phi$ yield the same results, as shown exemplarily for $\Delta\Phi = 0°$ in Fig. 6(a).

With spin-orbit coupling ($\lambda = 0.2\,t$), the collinear ferromagnets exhibit a spin Hall effect [cf. Fig. 6(b)] which is equal for both collinear phases ($\theta = 0°, 180°$) since the spin Hall effect in ferromagnets is not affected by reversal of the magnetic moments [42]. Besides, the shape of the signal is only slightly deformed and the curves are mainly shifted by $\Delta\theta \approx 13°$. This can be seen by comparing the positions of the local extrema in Figs. 6(a) and 6(b). This angle is the same critical angle $\Delta\theta_c$ that we revealed for $\lambda = 0.2\,t$ in Ref. [34].

As explained before, the anomalous Hall effect is absent for this noncoplanar (radial-type) texture characterized by $\theta_c = 90° + \Delta\theta_c$. In this case, the virtual texture is coplanar and the effective spin-orbit coupling according to Eq. (10) is compensated. Therefore, the noncoplanar system behaves as if it was effectively coplanar due to the equivalence of spin-orbit interaction and out-of-plane tilting of the magnetic texture that compensate each other, here.

To corroborate this, we compare the spin Hall signal as a function of E_{F} for this critical angle [black curve in Fig. 6(c)] with the one of the coplanar configuration [red curve in Fig. 6(c)] that we have already shown before. As visible, the spin Hall signal characterized by this critical angle with spin-orbit coupling is the same as the one of the coplanar

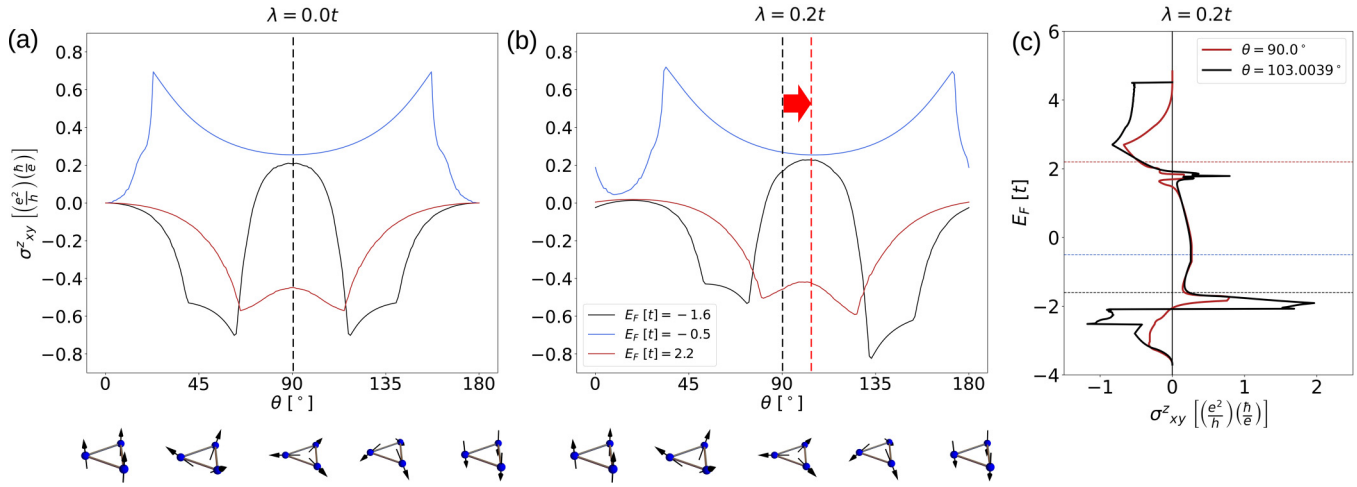

FIG. 6. Spin Hall conductivity under out-of-plane rotation of the radial-type magnetic texture ($\Delta\Phi = 0°$). (a) The spin Hall signal is symmetric with respect to $\theta = 90°$ if spin-orbit coupling is not considered. (b) If spin-orbit interaction is taken into account, the curves of (a) are slightly deformed and mainly shifted by the critical angle $\Delta\theta_c \approx 13°$, as well. (c) The spin Hall conductivity as a function of E_F for the radial-type arrangement (with spin-orbit coupling) that is characterized by the critical out-of-plane orientation (black curve) is identical to the signal of the coplanar configuration without spin-orbit coupling [cf. black curve from Fig. 3(b)]. The red curve is the same as the red curve in Fig. 3(b) for the coplanar texture with spin-orbit coupling. The horizontal lines indicate the values of the Fermi level chosen in (a) and (b).

configuration where spin-orbit interaction is neglected [black curve in Fig. 3(b)].

This explicitly proves that tilting the texture has the same effect as spin-orbit coupling in this model.

IV. CONCLUSION

In summary, we have identified two mechanisms determining the spin Hall signal. We showed via tight-binding calculations that the main contribution is a pure spin current that originates from the coplanar magnetic background texture. Besides, spin-orbit coupling is equivalent to an out-of-plane tilting of the magnetic moments and thereby generates an asymmetry in the spin polarization with respect to the quantization axis perpendicular to the kagome plane. Thus, with spin-orbit interaction a spin-polarized current is flowing as well that reduces the spin Hall signal of the pure spin current effectively.

Therefore, noncollinear kagome antiferromagnets have the potential for applications in spintronic devices where they might be utilizable as alternative generators for spin currents and spin-polarized currents in analogy to collinear antiferromagnets and ferromagnets, respectively (cf. Fig. 1).

Besides, our results might be insightful for the experimental observation of the spin Hall effect in manganese compounds with a positive vector spin chirality like Mn_3Ir. In this material, the anomalous Hall effect was predicted theoretically seven years ago [27,28], but it has not been measured up to now. The reason is that domains with different phases that we characterize by $\Delta\Phi = 0°$ and 180° occur in that material [43]. The anomalous Hall effect is allowed in both phases but both signals compensate each other due to their opposite sign [27,34]. However, our findings show that the spin Hall signal would be the same for both phases and therefore there could be the possibility to measure the spin Hall effect without the need to prepare single-domain samples.

ACKNOWLEDGMENTS

This work is supported by CRC/TRR 227 of Deutsche Forschungsgemeinschaft (DFG).

O.B. performed the tight-binding calculations with the help of B.G. O.B. wrote the manuscript with significant input from all authors. O.B. prepared the figures. All authors discussed the results. B.G. and I.M. planned and supervised the project.

[1] K. Sadasivuni, A. Y. Al Haddad, H. Javed, W. Yoon, and J.-J. Cabibihan, Strain, pressure, temperature, proximity, and tactile sensors from biopolymer composites, in *Biopolymer Composites in Electronics* (Elsevier, Amsterdam, 2017), pp. 437–457.

[2] M. I. D'yakonov and V. I. Perel, Current-induced spin orientation of electrons in semiconductors, Phys. Lett. A **35**, 459 (1971).

[3] M. I. D'yakonov and V. I. Perel, Spin orientation of electrons associated with the interband absorption of light in semiconductors, Soviet J. Exper. Theor. Phys. **33**, 1053 (1971).

[4] I. Žutić, J. Fabian, and S. D. Sarma, Spintronics: Fundamentals and applications, Rev. Mod. Phys. **76**, 323 (2004).

[5] V. Baltz, A. Manchon, M. Tsoi, T. Moriyama, T. Ono, and Y. Tserkovnyak, Antiferromagnetic spintronics, Rev. Mod. Phys. **90**, 015005 (2018).

[6] R. Duine, An alternating alternative, Nat. Mater. **10**, 344 (2011).

[7] J. Sinova and I. Žutić, New moves of the spintronics tango, Nat. Mater. **11**, 368 (2012).

[8] J. E. Hirsch, Spin Hall Effect, Phys. Rev. Lett. **83**, 1834 (1999).

[9] H. Ohno, Making nonmagnetic semiconductors ferromagnetic, Science **281**, 951 (1998).

[10] S. Pearton, C. Abernathy, M. Overberg, G. Thaler, D. Norton, N. Theodoropoulou, A. Hebard, Y. Park, F. Ren, J. Kim *et al.*, Wide band gap ferromagnetic semiconductors and oxides, J. Appl. Phys. **93**, 1 (2003).

[11] V. Dediu, M. Murgia, F. Matacotta, C. Taliani, and S. Barbanera, Room temperature spin polarized injection in organic semiconductor, Solid State Commun. **122**, 181 (2002).

[12] D. A. Pejaković, C. Kitamura, J. S. Miller, and A. J. Epstein, Photoinduced Magnetization in the Organic-Based Magnet $Mn(TCNE)_x \cdot y(CH_2Cl_2)$, Phys. Rev. Lett. **88**, 057202 (2002).

[13] A. Goldman, V. Vas'ko, P. Kraus, K. Nikolaev, and V. Larkin, Cuprate/manganite heterostructures, J. Magn. Magn. Mater. **200**, 69 (1999).

[14] J. Schliemann, Spin Hall effect, Int. J. Mod. Phys. B **20**, 1015 (2006).

[15] J. Sinova, S. O. Valenzuela, J. Wunderlich, C. H. Back, and T. Jungwirth, Spin Hall effects, Rev. Mod. Phys. **87**, 1213 (2015).

[16] Y. K. Kato, R. C. Myers, A. C. Gossard, and D. D. Awschalom, Observation of the spin Hall effect in semiconductors, Science **306**, 1910 (2004).

[17] T. Kimura, Y. Otani, T. Sato, S. Takahashi, and S. Maekawa, Room-Temperature Reversible Spin Hall Effect, Phys. Rev. Lett. **98**, 156601 (2007).

[18] L. Liu, C.-F. Pai, Y. Li, H. Tseng, D. Ralph, and R. Buhrman, Spin-torque switching with the giant spin Hall effect of tantalum, Science **336**, 555 (2012).

[19] J. C. Slonczewski, Current-driven excitation of magnetic multilayers, J. Magn. Magn. Mater. **159**, L1 (1996).

[20] L. Berger, Emission of spin waves by a magnetic multilayer traversed by a current, Phys. Rev. B **54**, 9353 (1996).

[21] A. Khvalkovskiy, D. Apalkov, S. Watts, R. Chepulskii, R. Beach, A. Ong, X. Tang, A. Driskill-Smith, W. Butler, P. Visscher *et al.*, Basic principles of STT-MRAM cell operation in memory arrays, J. Phys. D **46**, 074001 (2013).

[22] H. Reichlova, T. Janda, J. Godinho, A. Markou, D. Kriegner, R. Schlitz, J. Zelezny, Z. Soban, M. Bejarano, H. Schultheiss *et al.*, Imaging and writing magnetic domains in the noncollinear antiferromagnet Mn_3Sn, Nat. Commun. **10**, 5459 (2019).

[23] S. A. Siddiqui, J. Sklenar, K. Kang, M. J. Gilbert, A. Schleife, N. Mason, and A. Hoffmann, Metallic antiferromagnets, J. Appl. Phys. **128**, 040904 (2020).

[24] R. Cheng, M. W. Daniels, J.-G. Zhu, and D. Xiao, Ultrafast switching of antiferromagnets via spin-transfer torque, Phys. Rev. B **91**, 064423 (2015).

[25] L. Šmejkal, Y. Mokrousov, B. Yan, and A. H. MacDonald, Topological antiferromagnetic spintronics, Nat. Phys. **14**, 242 (2018).

[26] Y. Zhang, Y. Sun, H. Yang, J. Železny, S. P. P. Parkin, C. Felser, and B. Yan, Strong anisotropic anomalous Hall effect and spin Hall effect in the chiral antiferromagnetic compounds Mn_3X (X = Ge, Sn, Ga, Ir, Rh, and Pt), Phys. Rev. B **95**, 075128 (2017).

[27] H. Chen, Q. Niu, and A. H. MacDonald, Anomalous Hall Effect Arising from Noncollinear Antiferromagnetism, Phys. Rev. Lett. **112**, 017205 (2014).

[28] J. Kübler and C. Felser, Non-collinear antiferromagnets and the anomalous Hall effect, Europhys. Lett. **108**, 67001 (2014).

[29] S. Nakatsuji, N. Kiyohara, and T. Higo, Large anomalous Hall effect in a non-collinear antiferromagnet at room temperature, Nature (London) **527**, 212 (2015).

[30] A. K. Nayak, J. E. Fischer, Y. Sun, B. Yan, J. Karel, A. C. Komarek, C. Shekhar, N. Kumar, W. Schnelle, J. Kübler *et al.*, Large anomalous Hall effect driven by a nonvanishing Berry curvature in the noncolinear antiferromagnet Mn_3Ge, Sci. Adv. **2**, e1501870 (2016).

[31] N. Kiyohara, T. Tomita, and S. Nakatsuji, Giant Anomalous Hall Effect in the Chiral Antiferromagnet Mn_3Ge, Phys. Rev. Appl. **5**, 064009 (2016).

[32] Y. Zhang, J. Železny, Y. Sun, J. Van Den Brink, and B. Yan, Spin Hall effect emerging from a noncollinear magnetic lattice without spin–orbit coupling, New J. Phys. **20**, 073028 (2018).

[33] M. Seemann, D. Ködderitzsch, S. Wimmer, and H. Ebert, Symmetry-imposed shape of linear response tensors, Phys. Rev. B **92**, 155138 (2015).

[34] O. Busch, B. Göbel, and I. Mertig, Microscopic origin of the anomalous Hall effect in noncollinear kagome magnets, Phys. Rev. Research **2**, 033112 (2020).

[35] C. Herring, *Magnetism: A Treatise on Modern Theory and Materials. 4. Exchange Interactions among Itinerant Electrons* (Academic, New York, 1966).

[36] X. Zhou, J.-P. Hanke, W. Feng, F. Li, G.-Y. Guo, Y. Yao, S. Blügel, and Y. Mokrousov, Spin-order dependent anomalous Hall effect and magneto-optical effect in the noncollinear antiferromagnets Mn_3XN with X = Ga, Zn, Ag, or Ni, Phys. Rev. B **99**, 104428 (2019).

[37] N. Nagaosa, J. Sinova, S. Onoda, A. H. MacDonald, and N. P. Ong, Anomalous Hall effect, Rev. Mod. Phys. **82**, 1539 (2010).

[38] D. Fruchart and E. F. Bertaut, Magnetic studies of the metallic perovskite-type compounds of manganese, J. Phys. Soc. Jpn. **44**, 781 (1978).

[39] Note that σ^z_{xy} is negative for the chosen fixed occupation number.

[40] Note that their dependence can also be more complicated.

[41] B. F. Miao, S. Y. Huang, D. Qu, and C. L. Chien, Inverse Spin Hall Effect in a Ferromagnetic Metal, Phys. Rev. Lett. **111**, 066602 (2013).

[42] D. Tian, Y. Li, D. Qu, S. Y. Huang, X. Jin, and C. L. Chien, Manipulation of pure spin current in ferromagnetic metals independent of magnetization, Phys. Rev. B **94**, 020403(R) (2016).

[43] C. Ulloa and A. S. Nunez, Solitonlike magnetization textures in noncollinear antiferromagnets, Phys. Rev. B **93**, 134429 (2016).